Cryo-electron tomography: The challenge of doing structural biology in situ

Vladan Lučić, Alexander Rigort, and Wolfgang Baumeister

Max-Planck-Institute of Biochemistry, Am Klopferspitz 18, 82152 Martinsried, Germany

Electron microscopy played a key role in establishing cell biology as a discipline, by producing fundamental insights into cellular organization and ultrastructure. Many seminal discoveries were made possible by the development of new sample preparation methods and imaging modalities. Recent technical advances include sample vitrification that faithfully preserves molecular structures, three-dimensional imaging by electron tomography, and improved image-processing methods. These new techniques have enabled the extraction of high fidelity structural information and are beginning to reveal the macromolecular organization of unperturbed cellular environments.

Introduction

For a long time, scientists have attempted to understand biological phenomena through studies of the molecules that make up a living cell. This reductionist approach of isolating and purifying molecules for structural and functional studies has been enormously successful. The atomic resolution structures of DNA and proteins such as myoglobin, hemoglobin, and lysozyme were early triumphs of the emerging discipline of molecular structural biology because these structures provided insights into molecular functions.

Despite these achievements, in recent years it has become apparent that discrete biological functions can only rarely be attributed to individual molecules. Nearly every major process in a cell is performed by molecular assemblies that form functional modules and many biochemical pathways require a distinctly nonrandom spatial organization of their components to proceed efficiently (Alberts, 1998; Hartwell et al., 1999). Recent years have witnessed an explosion in the amount of information about the identity of the molecular players involved in cellular processes. Cellular proteomes have been comprehensively analyzed by genomics and mass spectrometry–based proteomics. Putative large-scale interaction networks determined by methods such as two-hybrid screening or affinity purification in conjunction with mass spectrometry (Aloy and Russell 2004) have helped assign proteins to macromolecular complexes and order them into plausible biochemical pathways (Gavin et al., 2002; Tong et al., 2004; Walther and Mann 2010). However, many of these assignments are tentative and need to be confirmed by structural methods.

Some molecular assemblies are held together by interactions that are strong enough to withstand the rigors of purification. Such complexes with stable quaternary structures are often amenable to studies using traditional structural biology methods such as x-ray crystallography and single-particle electron microscopy. However, many assemblies exist only transiently, or are not stable enough to be studied in vitro. Their structure determination is much more challenging because they disintegrate when subjected to standard isolation methods involving cell disruption and fractionation. Furthermore, it is often difficult to reconstitute molecular assemblies in vitro because the diverse and crowded cellular environment cannot be easily mimicked. In situ structure determination requires the development of methods allowing structural studies to be performed within unperturbed cells. These methods must be capable of determining the precise spatial relationships between components of unstable and transient molecular assemblies under physiological conditions. A "visual proteomics" approach, i.e., proteomics based on imaging (Nickell et al., 2006), adds a new dimension to the established methods of mass spectrometry–based proteomics.

Electron microscopy (EM) can bridge the gap between ultrastructural compartmentalization and the structural analysis of molecular inhabitants of the cell, at a nanometer-length scale (termed "mesobiology" in Ball, 2003) by providing high resolution 3D images (tomograms) of cellular landscapes. The combination of EM with cryo-techniques, termed cryo-electron tomography (cryo-ET, see Box 1), enables the visualization of frozen hydrated biological samples unadulterated by harmful preparation methods. Cryo-ET is based on old ideas, but now the time has come to provide a structural picture of the undisturbed macromolecular organization inside cells (Robinson et al., 2007). This review begins with a section that puts the recent developments of sample preparation methods into a historical perspective.

The Rockefeller University Press
J. Cell Biol. Vol. 202 No. 3 407–419
www.jcb.org/cgi/doi/10.1083/jcb.201304193

JCB 407

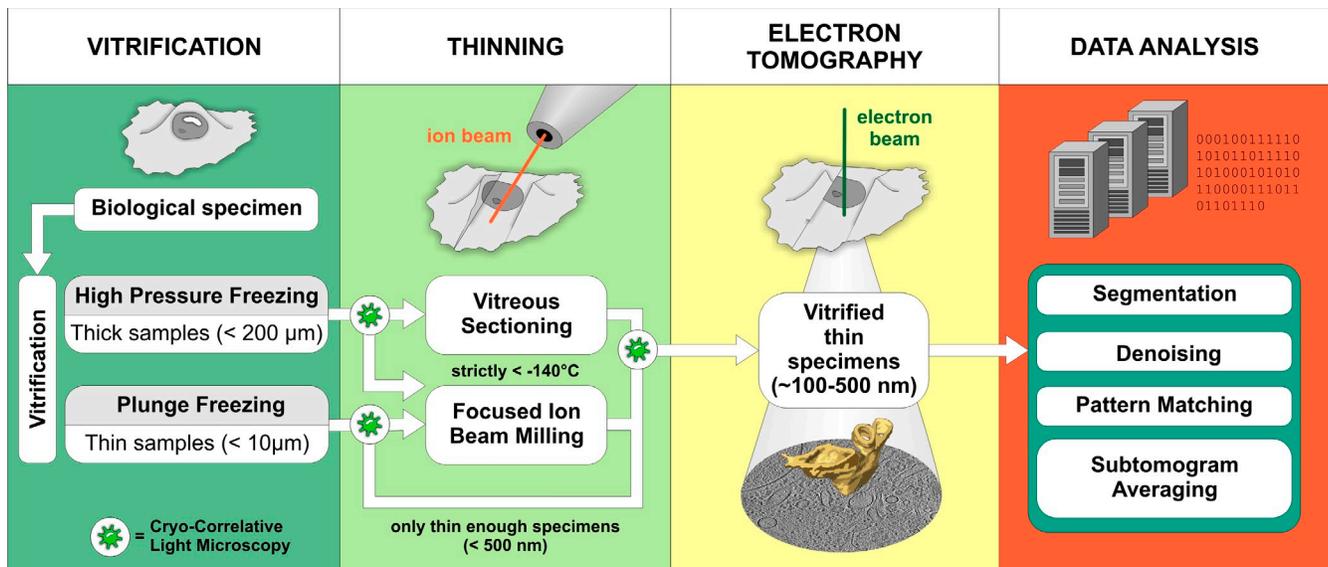| VITRIFICATION | THINNING | ELECTRON TOMOGRAPHY | DATA ANALYSIS |

Figure 1. Schematic representation of the cryo-ET workflow. Vitrification. The sample type usually dictates the vitrification method. Samples that are thin enough to be directly investigated by EM are commonly vitrified by plunge-freezing into a cryogen (such as liquid ethane at less than −160°C) where sufficiently fast cooling speeds are reached (Dubochet et al., 1988). High-pressure freezing combines rapid temperature decrease with the application of high pressure, which lowers the melting point of water. This allows vitrification of samples up to 200 μm in thickness, but cryo-protectants are often needed (Studer et al., 2008). Thinning. Due to a strong electron–matter interaction, samples thicker than 1 μm are virtually opaque to electrons and require thinning at cryo-conditions. Although vitreous sectioning is currently used more often, focused ion beam milling (FIB) is an emerging method with a great promise for the future (see Box 2). Electron tomography. 3D images of vitrified samples are produced by tomographic imaging (see Box 1 for more information). Data analysis. Computational methods are used to improve the resolution of structures visualized in tomograms and to aid in their molecular identification. Cryo-correlative light microscopy is an optional procedure that facilitates identification and navigation to target features in cryo-ET.

The cellular cryo-ET workflow is outlined in Fig. 1, basic technical details about electron imaging and tomography can be found in Box 1, and promising technical advances are described in Box 2. We then discuss the interpretation of tomograms with particular attention to molecular identification and highlight developments that will likely be important for the future of cellular cryo-ET of eukaryotic systems (see Gan and Jensen 2012 for a recent review covering other aspects of electron tomography).

The road to sample preparation in cryo-electron tomography

A short history of sample preparation. Electron microscopy played a fundamental role in establishing the discipline of cell biology, even though the origins of the field and the term "cell biology" date back to the nineteenth century (Carnoy 1884). The contribution of EM to cell biology is illustrated by the role of eminent electron microscopists, and Keith Porter in particular, in establishing this journal (Porter and Bennett 1981). The electron microscope was invented by Ernst Ruska in the 1930s, and its resolution soon surpassed that of the light microscope (Ruska 1979). Several technical developments during the following decades helped resolve the basic problems of imaging biological materials by EM.
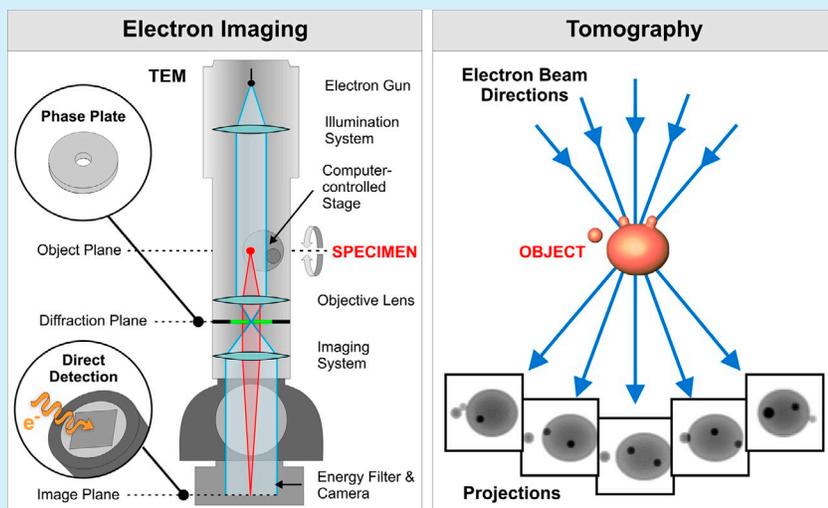
The development of the ultramicrotome (Porter and Blum 1953; Sjostrand 1953) with glass (Latta and Hartmann 1950) and diamond knives (Fernandez-Moran 1953) was arguably the most important advancement in enabling the preparation of sufficiently thin specimens (Afzelius and Maunsbach 2004). Resin embedding media such as methacrylate (Newman et al., 1949) gave samples the strength required for sectioning. Sample fixation by osmium tetroxide improved the preservation of cellular features and additional staining with heavy metals provided strong contrast. The electron irradiation of samples was reduced to tolerable levels by instrument improvements such as the introduction of the condenser aperture.

Subsequent technical advancements led to major discoveries, but the basic sample preparation workflow comprising chemical fixation, heavy-metal staining, dehydration, embedding, and sectioning remained the same. Studies that carefully compared different preparation methods identified artifacts and in doing so stimulated further improvements (Maunsbach and Afzelius 1999; Afzelius and Maunsbach 2004). However, it became evident that these harsh procedures bore the risk of altering the structure of biological samples, which could lead to misconceptions about cellular organization (Heuser 2002). The lack of external standards and uncertainty about the faithful preservation of biological structures remained problematic, and EM was increasingly perceived as an expensive, artifact-prone method requiring long training periods (Geuze 1999). Nevertheless, this method has been central to our understanding of cellular organization and ultrastructure, and currently new modalities for imaging large volumes are under development (Denk and Horstmann 2004).

Freezing, a well-known method for stabilizing biological material, was used as the initial step in an EM preparation approach that is followed by sample dehydration at low temperature (freeze-drying) and embedding to allow sectioning at room temperature (Müller 1957). Artifacts associated with this procedure inspired the development of cryo-methods such as freeze-fracture and superficial freeze-drying (etching) of samples at

Box 1. Principles of electron tomography

| Electron Imaging | Tomography |

Electron imaging.

Image contrast arises primarily because of variations in the density within a sample. Because unstained biological material essentially consists of atoms of low atomic number, the contrast and consequently the SNR is generally low in cryo-ET.

Phase-contrast dominates in images of unstained samples. In cryo-ET it is normally induced by slight negative defocusing (underfocusing). Underfocus phase-contrast is caused by an interference effect that modulates both low and high frequencies (see Reimer and Kohl (2008) for details). It is mathematically described by the contrast transfer function (CTF), an oscillating function in spatial frequencies that has regions of inverted contrast, effectively limiting the range of spatial frequencies in tomograms. Increasing underfocus increases apparent contrast but decreases resolution (see examples in Fig. 2 of Vanhecke et al., 2011).

Electron interaction with matter results in elastic and inelastic electron scattering. Electrons that interact with atomic nuclei scatter elastically; they are used for imaging because they are well localized and contain high resolution information. Inelastically scattered electrons have poor localization and coherence and therefore do not contribute to high resolution information. When imaging thick samples (above 250–300 nm in thickness) it is crucial that most of the inelastically scattered and multiple scattered electrons are removed by an energy filter before they reach the electron detector. Nevertheless, these electrons deposit part of their energy in the sample and can cause sample damage, thus limiting the electron dose available for imaging and the SNR. Increasing sample thickness further decreases the available electron dose, which lowers the achievable resolution and prevents imaging samples thicker than 1 µm.

Tomography.

In electron tomography, a set of electron micrographs (tilt series) is acquired at different angular orientations of the sample. Tilting of the sample is accomplished by rotation of a computer-controlled specimen stage. Each electron micrograph is a projection through the sample where structural information is superimposed in the direction of the electron beam. This superposition obscures structural details in the individual images. Tilt series images are then aligned and computationally merged into a 3D image (tomogram), thus separating the superimposed structures. In contrast to confocal light microscopy, where images are acquired as successive z-slices of a sample, in electron tomography, z-slices can be computationally extracted only after reconstruction of a tomogram.

Typically, a specimen is tilted around a fixed axis. Physical restrictions of the instrument and sample thickness usually limit the tilt range to ±60–70°, resulting in an incomplete set of projections and missing information. The maximum attainable isotropic resolution depends on the sample size and the number of projections, and is determined from Crowther's criterion (Crowther et al., 1970). Upon reconstruction, this missing information (named the "missing wedge" due to its characteristic shape in Fourier space, see Fig. 4 in Lučić et al., 2005a) causes elongation in the electron-beam direction and other distortions. In principle, the commonly used fixed-angular-increment tilting scheme is not the best one (Saxton et al., 1984), but it appears to be the most robust in the presence of noise. Cryo-ET has to reconcile the need to maximize the number of projections with the requirement that all of the images have sufficient contrast to allow alignment, while keeping the cumulative dose low.

The development of procedures for automated tilt series acquisition was a decisive step that made cryo-ET of vitrified biological samples practical (Dierksen et al., 1992; Koster et al., 1992, 1997) and led to rapid progress of this technique (Mahamid and Baumeister 2012). These procedures use areas adjacent to the feature of interest to correct for positioning and focusing errors resulting from the mechanical imperfections of the EM stage, and consequently ensure that almost all of the allowed electron dose is spent on data acquisition.

lower temperatures (Steere 1957; Moor et al., 1961). The metal replicas obtained subsequently produce strong contrast and allow for limited 3D visualization by EM, but their granularity limits resolution. Freeze-fracture and freeze-etching produced superior structural preservation and at the time were considered to be artifact free. These methods provided definite answers about the basic architecture of biological membranes and the mode of interaction between lipids and membrane proteins (Branton 1971; Verkleij and Ververgaert 1978). In combination with quick freezing, this method delivered images of fast biological processes, such as synaptic vesicle release (Heuser et al., 1979).

Imaging hydrated samples in EM avoids dehydration-induced structural alterations such as flattening and collapse. An early approach using a hydration chamber placed inside the column of an electron microscope demonstrated the importance of full sample hydration for the preservation of high resolution information (Matricardi et al., 1972). Despite serving as a successful proof of concept, this hydration chamber was not developed further because it was cumbersome to operate. Furthermore, the movement of proteins in solution and subcellular components makes this approach incompatible with imaging modalities such as electron tomography, which require that the sample under scrutiny does not move during the extended time period required to acquire a tomographic image series.
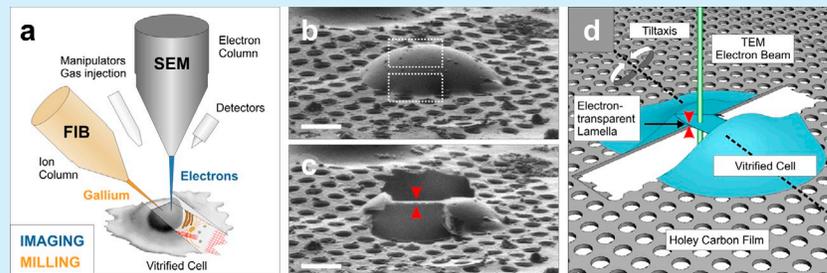
Complete vitrification of aqueous solutions, that is freezing that avoids ice crystal formation, was first achieved by jet-freezing of micrometer-sized droplets (Bruggeller and Mayer 1980). Currently, vitrification is achieved either by plunge-freezing (Dubochet et al., 1988) or high-pressure freezing (Studer et al., 2008), depending on the sample thickness (Fig. 1). High-pressure frozen samples may be dehydrated by freeze substitution, embedded in resin, sectioned, and imaged at room temperature (Hurbain and Sachse 2011). This procedure typically provides better preservation than methods based on chemical fixation and can reveal the detailed ultrastructure of large cellular volumes (Marsh et al., 2001). The term cryo-EM is sometimes misused; in our opinion it should be reserved for EM of

native (nonfixed, nonstained, fully hydrated) samples that are vitrified and then imaged by EM while still in the vitrified, fully hydrated, state.

Vitrification—state of the art of sample preservation. Vitrification occurs within microseconds, preventing the disruption of lipid membranes and changes in solvent concentration within the sample, artifacts that are usually caused by ice crystal growth. However, the sample has to remain below $-140°C$ at all times to avoid devitrification. Vitrified prokaryotic and eukaryotic cells are generally characterized by smooth and continuous membranes (Fig. 2). Their cytosolic material appears dense and well distributed, without signs of rearrangement and aggregation artifacts often associated with chemical fixation and dehydration. Vitrified biological material is observed directly, avoiding problems of heavy metal staining, where uneven stain distribution and the mixture of positive and negative contrast often complicate image interpretation.

Vitrified, fully hydrated in vitro samples show excellent structural preservation that allows reaching near-atomic resolution, as first demonstrated with catalase crystals (Taylor and Glaeser 1974). Hydrated, unstained samples are sensitive to electron irradiation because higher doses lead to progressive alterations of molecular structures (Glaeser 2008). Consequently, cryo-EM images have to be recorded at low electron exposures, limiting their signal-to-noise ratio (SNR). Thus, the high resolution information of images of vitrified samples is often buried in noise. This information can be retrieved by averaging-based noise reduction, which requires images of a large number of identical particles. When particles form 2D crystals, EM crystallography (Glaeser et al., 2007) is the method of choice for the 3D structure determination because it can provide atomic resolution structures (Fujiyoshi 2011). Alternatively, single-particle EM analysis requires randomly oriented particles and can reach resolutions better than 1 nm even for particles that lack symmetry (Henderson 2004). At this resolution, it becomes possible to directly detect helices, fit the atomic structures of individual domains or subunits into EM

Box 2.   Current technical developments

Focused ion beam (FIB) milling.
In this method, sample thinning is achieved by sputtering the specimen surface with gallium ions (panel a). Vitreous lamellae, cut at a shallow angle to the supporting grid and extending over tens of micrometers (panels c and d) were recently prepared from eukaryotic cells by cryo-FIB milling (Rigort et al., 2012a,c). Current development focuses on improving the reliability of the complete FIB-milling workflow and developing precise 3D targeting of low-copy number structures within large cellular volumes by correlative microscopy.

Phase plates.
Phase plates, which shift phases of some of the electrons in such a way that the CTF is partially corrected are currently under active development. They promise to enhance the contrast and allow imaging closer to focus, thus improving the high resolution information (Danev and Nagayama 2010). Several different conceptual types of phase plates have been proposed, but problems related to their manufacturing, durability, and integration into the EM column still await solutions.

Direct detection devices (DDDs).
In contrast to the charge-coupled device (CCD)–based detectors that are currently in widespread use, DDDs detect electrons directly and avoid blurring and distortions due to the generation and transfer of photons. Better transfer properties, stronger signal, and faster readout promise to make DDDs superior to steadily improving CCD cameras, albeit at the cost of a reduced lifetime (McMullan et al., 2009; Milazzo et al., 2011).

Dual-axis tomography.
Tilting around two tilt axes perpendicular to each other reduces missing wedge–induced distortions and improves information content. However, dual-axis tomography has rarely been used in cryo-ET due to the need to acquire an increased number of projections and difficulties with alignment. The increased sensitivity of DDDs is expected to alleviate these problems and enable the routine use of dual-axis tomography.

density maps, and to integrate this information with other methodologies ("hybrid methods"). This allows obtaining pseudo-atomic structures of complexes that are inaccessible to x-ray crystallography due to their size or biochemical properties. Currently, single-particle cryo-EM is the imaging method of choice for averaging-based approaches of repetitive structures (Frank 2002).

Whereas in vitro samples are thin (~50 nm), most eukaryotic cells exceed the thickness accessible to transmission electron microscopy (up to 0.5–1 µm), thus necessitating a thinning step under cryo-conditions (Fig. 1). Vitreous sectioning is a challenging method that yields thin sections of vitrified material, enabling images that contain high levels of detail (Al-Amoudi et al., 2004). However, vitreous sectioning leaves compression in the cutting direction, an artifact that is difficult to quantify and correct (McDowall et al., 1983; Al-Amoudi et al., 2005; Hsieh et al., 2006). A fundamentally different way to thin specimens uses focused ion beam (FIB) milling (see Box 2). Pilot studies have shown that cryo-FIB milling can indeed render regions of vitrified cells transparent enough for EM (Marko et al., 2007; Hayles et al., 2010; Rigort et al., 2010), promising to greatly extend the applicability of cellular cryo-ET. So far these studies have failed to detect significant artifacts and only subtle ion beam–induced alterations are expected to occur within a layer of 5–20 nm within the milled surfaces (Marko et al., 2006).

Between intact cells and high resolution

Sample choice and preparation have a strong influence on the level of detail that can be obtained in cryo-tomograms. Because sample thickness is inversely correlated to the
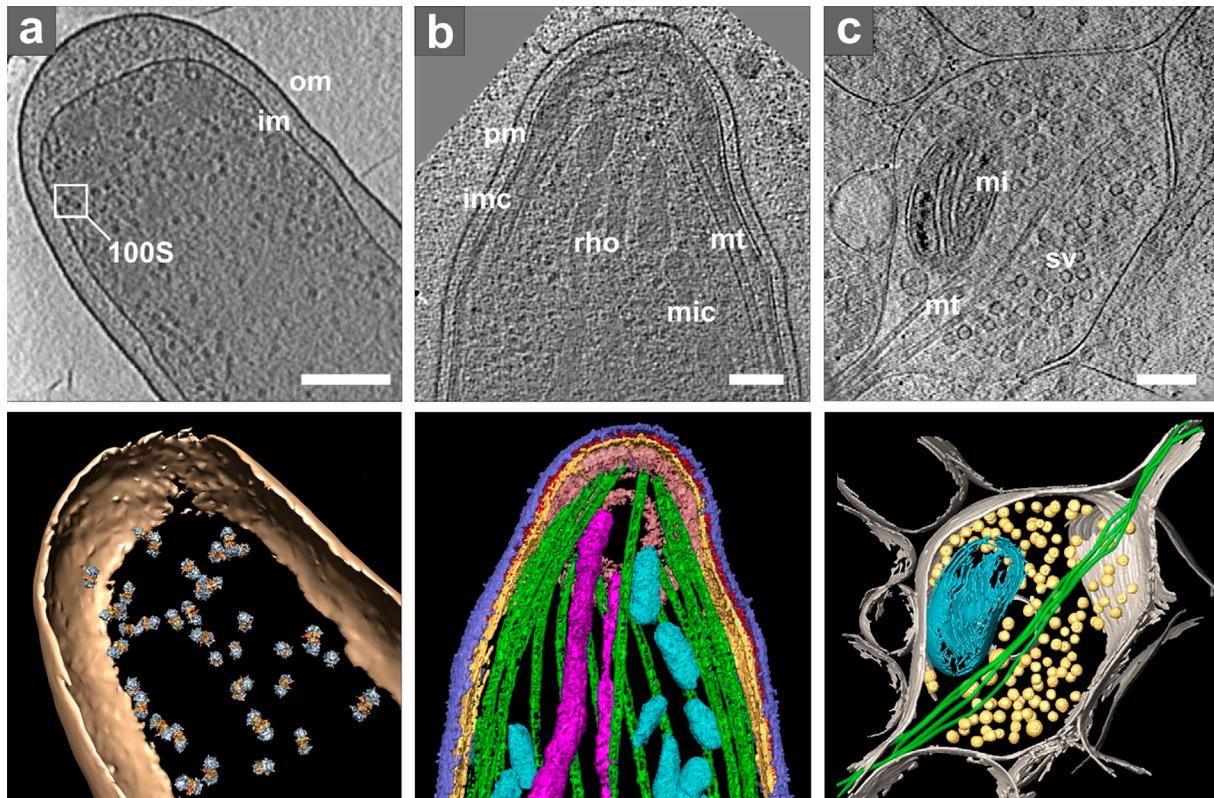
Figure 2. **Cryo-ET of intact cells.** (a) Intact *E. coli*. Top: tomographic slice. Bottom: isosurface representation with positions of template-matched ribosome pairs: om, outer membrane; im, inner membrane; inset shows one ribosome pair (100S). Bar, 200 nm. Modified from Ortiz et al. (2010). (b) *Plasmodium* organelles and the associated cytoskeleton. Top: tomographic slice. Bottom: surface rendering showing plasma membrane (pm, blue), inner membrane complex (imc, yellow), density between pm and imc (red), microtubules (mt, green), apical polar ring (pink), rhoptries (rho, violet), and micronemes (mic, cyan). Bar, 100 nm. Reproduced from Kudryashev et al. (2010b). (c) Presynaptic terminal visualized in vitrified dissociated neuronal culture at 15 days in vitro and thinned by FIB milling. Top: tomographic slice (courtesy of Y. Fukuda). Bottom: 3D visualization: plasma membrane (gray), microtubules (mt, green), mitochondrion (mi, cyan), and synaptic vesicles (sv, yellow). Bar, 200 nm.

achievable resolution (Box 1), cryo-tomograms of thick, intact cells are confined to the lower resolution range, whereas thin samples, such as cellular fractions and reconstituted systems, allow reaching higher resolution.

Cryo-tomograms of cellular samples contain information about a large number of molecular components in a single image, but this makes the identification of specific structures challenging. Here we review strategies that address these two basic problems: sample thickness and molecular identification.

Visual molecular identification in intact cells. The identification of structures in cryo-tomograms of intact cells is often limited to visual recognition of large features that can be clearly distinguished, including membranes, organelles, the cytoskeleton, and large complexes such as ribosomes (Fig. 2 a). Because the thin peripheral regions of cells provide good contrast, it is not surprising that the visualization of actin in the slime mold *Dictyostelium* marked the beginning of cellular cryo-tomography (Medalia et al., 2002). Further explorations aiming to reach deeper into cells identified several mammalian cell lines that possess extended thin regions accessible to cryo-ET (Garvalov et al., 2006; Cyrklaff et al., 2007; Sartori et al., 2007; Koning et al., 2008). Vitreous sectioning has allowed the investigations of structures located in the thickest parts of intact cells, such as the chromatin (Eltsov et al., 2008).

Fig. 2 b exemplifies cryo-ET of intact eukaryotic cells imaged in toto. This comprehensive study of the ultrastructure of the malaria-causing parasite *Plasmodium* identified the location of all of the major organelles and microtubules as well as numerous small filaments linking microtubules to the inner membrane (Kudryashev et al., 2010b). Several subsequent papers built upon this work. Notably, cryo-ET observations of the periphery of *Plasmodium*-infected and uninfected human erythrocytes revealed that the host–parasite interaction induces the reorganization of host actin cytoskeleton and establishment of the secretory system (Cyrklaff et al., 2011). Interference with actin remodeling and secretory activity was shown to impart protection against malaria (Cyrklaff et al., 2012), thus demonstrating the medical relevance of cryo-ET in situ observations.

The optimization of growth conditions to make cells suitable for cellular cryo-ET requires particular attention, especially for adherent cells that need to be grown on EM grids before vitrification. For example, individual neuronal axons and dendrites are relatively thin, but mature neurons in culture develop a dense network of processes that rapidly becomes prohibitively thick for imaging by cryo-ET. Consequently, neuronal cultures were investigated at early stages (Garvalov et al., 2006) or grown at low density (Lucić et al., 2007). Very recently, advances in FIB milling have made it possible to overcome this limitation

and image synapses situated within dense networks of mature neuronal cells (Fig. 2 c). The quality of these tomograms indicates that they are suitable for a quantitative assessment of synaptic complexes in intact cells.

Direct labeling and correlative light microscopy assist the identification of molecules by cryo-ET. Immunolabeling with electron-dense markers suitable for living cells tends to be restricted to proteins with extracellular epitopes because the cell permeabilization methods used to label intracellular proteins induce significant structural changes (Humbel et al., 1998). Nevertheless, immunolabeling works well for isolated cellular components. For example, spatial distribution of gold-labeled proteins undergoing transport through nuclear pores was visualized in cryo-tomograms of isolated nuclei (Beck et al., 2007).

Clonable labels for electron microscopy might allow the direct localization of proteins within the cell. Metal-binding proteins such as metallothionein and ferritin fused to cellular proteins act as nucleation sites for heavy atoms taken up from the surrounding medium (Mercogliano and DeRosier 2007; Nishino et al., 2007; Wang et al., 2011). Despite problems related to metal uptake, specificity, endogenous expression, and high concentrations of metal salts in the growth medium, initial attempts argue for the feasibility of metallothionein-based labeling (Diestra et al., 2009).

The widespread use of fluorescence microscopy has greatly advanced our understanding of cellular processes, but has also left many unanswered questions regarding the molecular and supramolecular architecture of cellular complexes. The combination of correlative light microscopy (LM) with cryo-ET allows imaging of the same feature over multiple-length scales. Correlative LM facilitates the search for features of interest, which otherwise can involve extensive scanning, as the field of view in cryo-ET is quite small in comparison to the size of a typical eukaryotic cell. Approaches combining LM with conventional EM preparation methods have clearly demonstrated the relevance of such techniques to cell biology (Koster and Klumperman 2003).

Successful applications of correlative LM and cryo-ET on sparse cultures of immature neurons (Garvalov et al., 2006) and endothelial cells (Braet et al., 2007) took advantage of strong visual cues provided by large cellular features, which allowed the straightforward orientation of the sample. The lack of distinct morphological features in complex, densely populated cell cultures requires a purely computational, coordinate transformation-based approach in order to determine the positions of fluorescently labeled structures in EM (Lucić et al., 2007).

LM imaging of vitrified samples (cryo-LM) assures that features of interest are identical during LM and EM imaging, thus overcoming possible alterations arising before and during vitrification. This imaging mode was made possible by the development of specialized holders mountable on standard light microscopes, ensuring that samples remain vitreous during extensive LM screening (Sartori et al., 2007; Schwartz et al., 2007; van Driel et al., 2009). However, current modular cryo-LM holders are only compatible with air objectives with long working distances, limiting the numerical aperture and thus the achievable resolution. Approaches facilitating a closer integration of light and electron imaging (Faas et al., 2013) or the use of higher numerical aperture objectives (Le Gros et al., 2009) require instrumentation modifications, and that have less flexibility and applicability than the modular approach.

Although molecular identification is unambiguous in fluorescence microscopy, only a few labeled species can be imaged simultaneously while their molecular environment remains invisible. Cryo-ET is complementary to fluorescence microscopy because it is based on the intrinsic modulation of density, provides a comprehensive picture of cellular components, and currently reaches at least an order of magnitude better resolution. The future adaptations of cryo-LM holders to single-molecule and super-resolution fluorescence imaging modes is expected to provide a much more precise localization of fluorescently labeled molecules, aiding in their correlative detection and identification in cryo-tomograms.

Linking structure with physiology. Readily available genetic manipulations can help identify molecules involved in the organization of cellular structures that can be visually identified in cryo-tomograms. Examples of this approach include bacterial cell envelopes (Hoffmann et al., 2008; Zuber et al., 2008; Kudryashev et al., 2009) and bacterial filaments (Salje et al., 2009). In the latter case, the precise location and arrangement of filamentous structures decisively implicated them in the movement of bacterial DNA.

It was long thought that prokaryotes do not have a cytoskeleton because it was not seen in chemically fixed and dehydrated samples. However, filamentous structures were visualized in vitrified bacteria and their molecular composition was identified in a comprehensive series of genetic studies (Li et al., 2007; Ingerson-Mahar et al., 2010; Pilhofer and Jensen 2013).

In other cases, the molecular identification of structures by genetic manipulation was less straightforward. For example, immuno-EM and fluorescent labeling were required to confirm the identity of arrays of bacterial chemotaxis receptors, even though these arrays were absent upon genetic deletion of the receptors (Zhang et al., 2007; Briegel et al., 2008).

In a similar manner, pharmacological manipulations that induce highly specific functional responses can be used to elucidate the composition and function of complexes observed in cryo-tomograms. Such an approach showed that initiating or modulating synaptic vesicle release results in a rearrangement of the presynaptic cytomatrix, the quantitative analysis of which led to a structural model of the release (Fig. 3; Fernández-Busnadiego et al., 2010).

The extension of the genetic approach to eukaryotes is bound to be more involved. Compensatory mechanisms activated in knock-out animals and multiple protein isoforms can present difficulties for the unequivocal molecular identification of structures visualized in cryo-tomograms (Fernández-Busnadiego et al., 2013). Nevertheless, structural alterations observed in the synapses of mutant mice led to a prediction about synaptic release deficit, which was subsequently confirmed by electrophysiological measurements.

Uncovering the information of tomograms by image processing

Computational approaches aimed at extracting the high resolution information present in cryo-tomograms have been rapidly
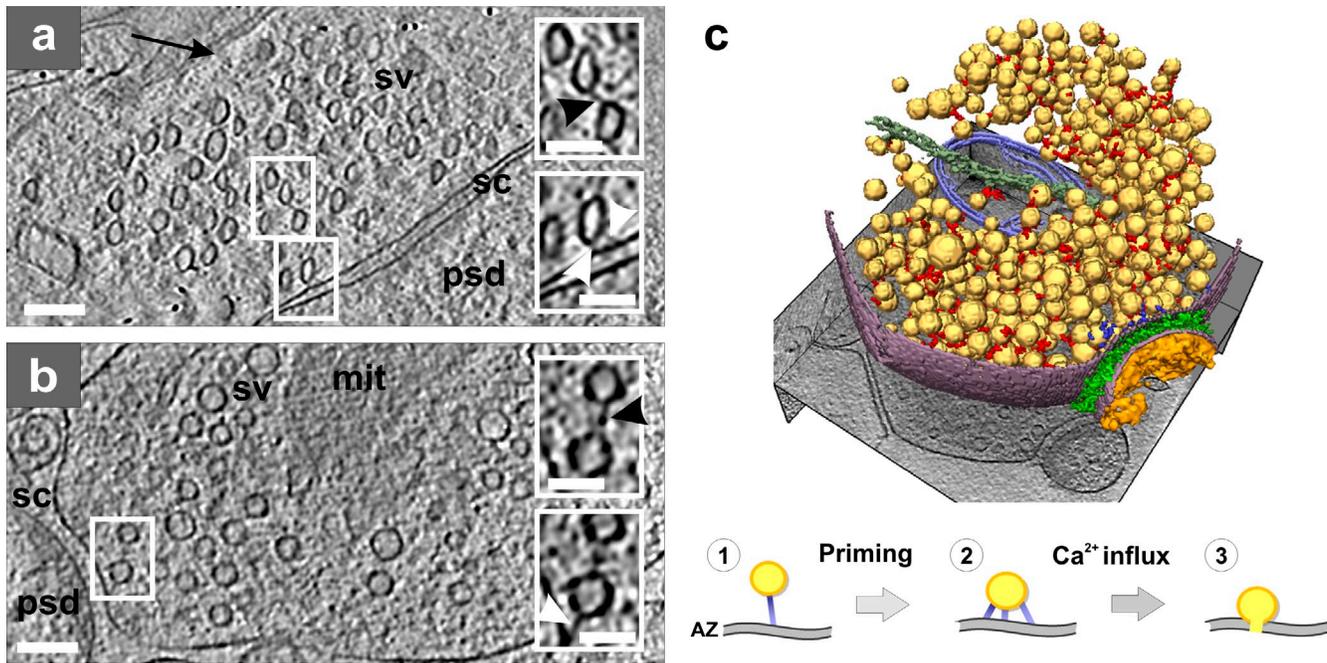
Figure 3. **Presynaptic cytomatrix.** (a) Tomographic slice of a synapse from a high-pressure frozen organotypic hippocampal slice, thinned by vitreous sectioning. Synaptic vesicles are compressed along the cutting direction (arrow). Top inset shows a connector (black arrowhead) that links two vesicles. Bottom inset shows tethers (white arrowheads) that link a vesicle to the active zone (AZ). (b) Tomographic slice of a synapse obtained from the synaptosomal cellular fraction. Top inset: connector linking two vesicles (black arrowhead). Bottom inset: tether linking a vesicle to the AZ (white arrowhead; same vesicles as in the top inset at another z-slice). (a and b) Synaptic vesicle (sv), mitochondrion (mit), synaptic cleft (sc), and postsynaptic density (psd). Bars: (main panels) 100 nm; (insets) 50 nm. (c) 3D rendering of a synaptosome; synaptic vesicles (yellow), connectors (red), tethers (blue), mitochondrion (light blue), microtubule (dark green), plasma membrane (purple), cleft complexes (green), and PSD (orange). Proposed structural model of the synaptic vesicle mobilization and release: initial tethering (1), primed vesicle (2), and release (3). Image copyright Fernández-Busnadiego et al. (2010).

expanding in recent years and are briefly summarized here (Fig. 1; see Fernandez [2012] for a more comprehensive review). These methods often complement each other, and their selection depends on the sample type and research goals.

Image restoration improves the quality of tomograms. Image denoising improves the SNR by reducing the noise while preserving the features of interest. Nonlinear anisotropic diffusion achieves this task by first detecting structures (edges) and then smoothing the image while preserving the edges (Frangakis and Hegerl 2001; Fernández and Li 2003). Nonlocal means filtering follows an approach based on the self-similarity of structures, which is particularly suited for filamentous structures (Rigort et al., 2012b).

Contrast-transfer-function correction restores the distorted high resolution information induced by image defocusing (Box 1). This requires that the defocus level is determined and corrected at each projection image of a tilt series. The defocus gradient present in tilted images and the low SNR make this a challenging task (Fernández et al., 2006). So far, the need for CTF correction in tomography has been somewhat underappreciated, but it will become mandatory to further improve the resolution, especially in combination with subtomogram averaging (discussed later).

Image segmentation separates structures of interest from the background. Structures of interest can be detected by manual segmentation, allowing their 3D visualization. The contours of structures are traced by hand on successive slices in the volume, an error-prone and time-consuming procedure that can be biased by subjective preferences.

However, quantitative morphological and statistical analysis requires objective and reproducible automated segmentation. Slice-by-slice membrane segmentation approaches predict membrane shapes at each slice based on previously segmented slices, local image properties, and external information (Moussavi et al., 2010; Martinez-Sanchez et al., 2011). Rigort et al. (2012b) described an actin segmentation procedure that uses template matching (see next section) to search for cylindrical structures with the dimensions of generic actin filaments (Fig. 4 a), thus providing a basis for the quantitative description of actin networks.

The detection of finer, nonuniform structures, such as membrane-bound complexes requires specialized approaches. The segmentation of synaptic–adhesion complexes was based on thresholding and connectivity (Lučić et al., 2005b), while presynaptic filaments were detected by combining this approach with some aspects of the watershed transform (Fig. 3 c; Fernández-Busnadiego et al., 2010).

Identification of molecular complexes by template matching. Large molecules and macromolecular complexes can be identified in tomograms by searching for a template representing the molecule or complex of interest. Templates are typically based on higher resolution structures obtained from x-ray crystallography or single-particle EM analysis. In an early example of in situ identification, ribosomes were successfully mapped in tomograms of the thin bacterium *Spiroplasma melliferum* (Ortiz et al., 2006).

In addition to location, template matching also shows the orientation of target structures. The determination of the relative
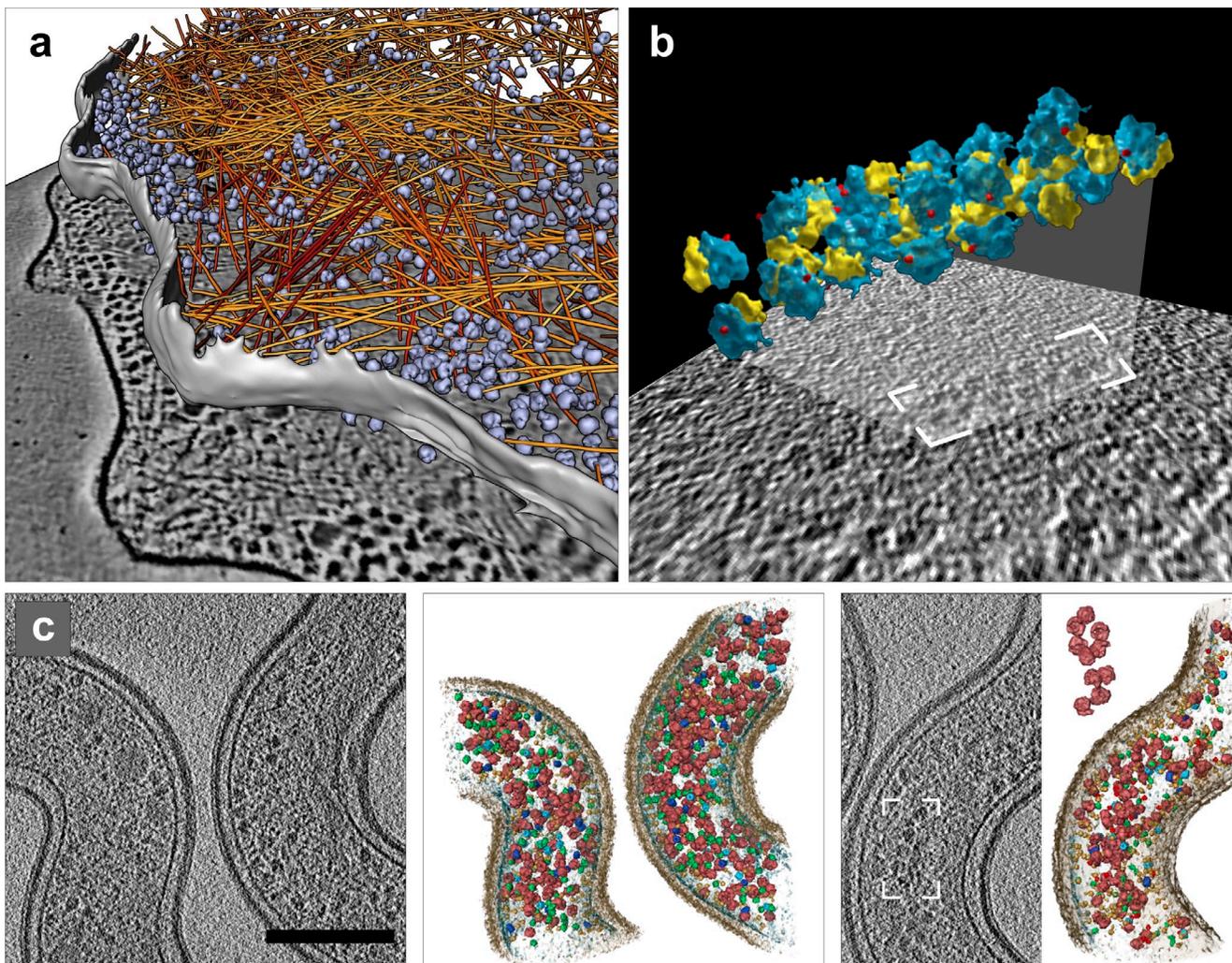
Figure 4. **Image processing: segmentation and template matching.** (a) Automated segmentation of actin filaments in *Dictyostelium discoideum*: actin filaments (yellow to red); ribosomes (blue). Reproduced with permission from Rigort et al. (2012b); copyright Elsevier, Inc. (b) Polyribosomes from intact human glioma cells identified by template matching. Modified with permission from Brandt et al. (2010); copyright Elsevier, Inc. (c) Protein identification using multiple template matching in intact *Leptospira interrogans*. Tomographic slices and 3D visualization of identified proteins of nonstimulated (left) and antibiotics-treated cells (right), ribosomes (red), GroEL (light blue), GroEL/ES (dark blue), and RNA polymerase II (green). Bar, 200 nm. Reprinted by permission from Macmillan Publishers Ltd: *Nature Methods* (Beck et al., 2009); copyright 2009.

orientations and distances between ribosomes and their nearest neighbors demonstrates the potential of structural biology in situ. Dimers of ribosomes in the hibernating state were unambiguously identified in intact *Escherichia coli* cells under conditions of nutritional stress (Fig. 2 a; Ortiz et al., 2010). These dimers represent a reversible state of quiescence, as they disappeared when the growth medium was replenished. In protrusions of intact glial cells, ribosomes engaged in active translation (polysomes) were visualized at the baseline condition, but this organization was lost after a treatment known to stop translation and dissociate polysomes (Fig. 4 b; Brandt et al., 2010). These studies exemplify the power of cryo-ET in situ, as the flexible nature of ribosome assemblies poses a problem for structural methods that rely on repetitive structures, such as single-particle analysis. In both studies, the structural differences between ribosomes in different functional states were explored by subtomogram averaging.

The template-matching examples mentioned above benefited from the strong inherent contrast that ribosomes possess in cryo-tomograms. Because most proteins have lower contrast, validation of template matching becomes an important task. The challenge is to convert the template-matching score that is obtained at all positions within a tomogram to one of the two expected outcomes (hit or miss). Beck et al. (2009) derived a statistical scoring function and assessed its performance for identification of 200–2,000 kD-sized proteins (Fig. 4 c). The applicability of template matching is currently limited to large protein complexes, but it is expected to improve in the near future as the fidelity of cryo-tomograms increases.

Increasing resolution by subtomogram averaging. In subtomogram averaging, a higher resolution structure of a particle (protein or a protein complex) is obtained by averaging 3D volumes extracted from tomograms. The procedure is conceptually similar to single-particle EM analysis; at each
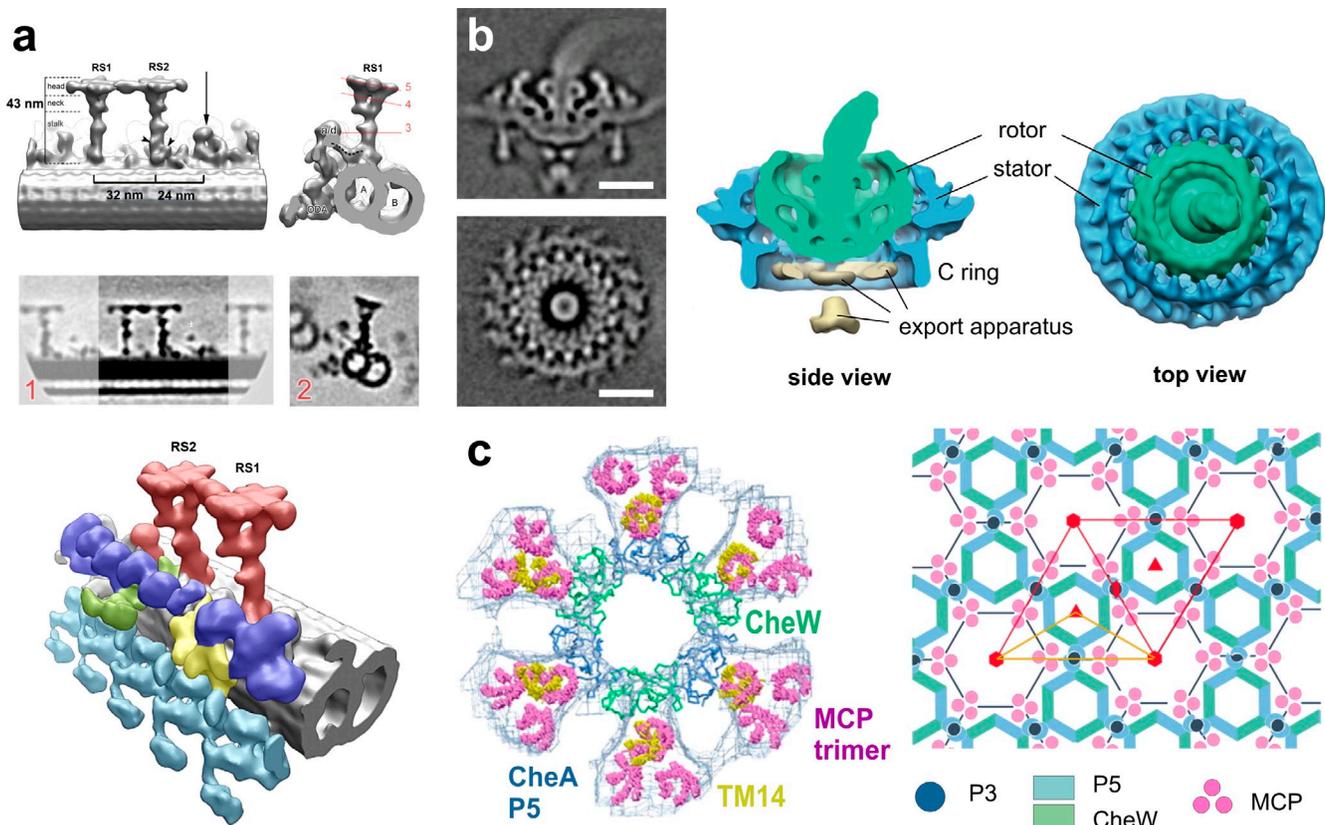
Figure 5. **Image processing: subtomogram averaging.** (a) Isolated *C. reinhardtii* axoneme. Top row: surface renderings of the density map obtained by averaging radial spokes (RS). Middle row: tomographic slices of the above density map. Bottom: surface renderings of the overall 3D structure: microtubule doublet (gray), outer dynein arms (turquoise), inner dynein arms (IDA, blue), the intermediate and light chains of IDAs (yellow), the dynein regulatory complex (green), and the radial spokes (red). RS1, radial spoke 1; RS2, radial spoke 2. Image copyright Pigino et al. (2011). (b) Flagellar motor of intact *Borrelia*. Left: tomographic slices of the averaged density map. Right: 3D isosurface views of the motor. Bars, 25 nm. Reproduced from Liu et al. (2009) with permission from the American Society for Microbiology. (c) Bacterial chemosensory receptors. Left: superposition of one ring of the crystal structure (P5 blue, CheW green) with its six receptor dimers (TM14, yellow) on the EM map (blue mesh) with its previously fit 18 receptor dimers (pink). Right: the arrangement of the receptor array produces P6 point symmetry (red; the asymmetric unit yellow). Image copyright Briegel et al. (2012).

iteration the angular orientation of particle images is determined based on an existing 3D structure (alignment), and then used to generate an improved structure. The alignment step in subtomogram averaging is more involved because it is done in 3D and has to account for the missing wedge (Box 1; Förster et al., 2005).

Thin, isolated systems that have periodic features are ideally suited for subtomogram averaging. These include microtubule-based systems, such as the centrioles (Guichard et al., 2012; Li et al., 2012) and eukaryotic flagella. Cryo-ET of flagella has yielded a series of publications providing detailed structures of flagellar components including the doublet microtubules (Nicastro et al., 2011), the dynein arms (Bui et al., 2009), the dynein regulatory complex (Heuser et al., 2009), and the radial spokes (Fig. 5 a; Lin et al., 2011; Pigino et al., 2011; Barber et al., 2012), thus bringing the field significantly closer to a molecular understanding of flagellar movement.

Vitreous sectioning yields very thin samples, which facilitates subtomogram averaging. Still, problems associated with the unpredictable degree of sample compression may restrict the usefulness of this preparation technique to rigid complexes such as ribosomes (Al-Amoudi et al., 2007; Pierson et al., 2011).

There is a great need to extend subtomogram averaging to tomograms of intact cells, in order to obtain 3D structures of molecules in situ. For example, the nuclear pore complex is a large protein assembly that is difficult to investigate by other structural biology methods. Averaging individual pores from tomograms of intact fibroblast cells yielded the structure of the complex, revealing new higher eukaryote-specific features (Maimon et al., 2012). Determining the structure of the *Borrelia* flagellar motor in situ was quite labor intensive because only a limited number of motors were present in each tomogram, necessitating large-scale data acquisition. Two complementing studies determined the precise localization of several proteins within the complex (Liu et al., 2009; Kudryashev et al., 2010a; see Fig. 5 b). Other applications of in situ subtomogram averaging have been recently reviewed in Briggs, 2013.

Future developments are expected to continue in different directions. First, the pseudo-atomic structures of larger complexes can be generated by combining subtomogram averaging of the whole complex with x-ray crystallography of its components, as done for bacterial chemoreceptors (Fig. 5 c; Briegel et al., 2012; Liu et al., 2012). Second, distinct functional states of a complex of interest, manifested by its conformational heterogeneity, can be discerned by 3D classification (Förster et al., 2008), as pursued for nucleotide binding–induced dynein conformational changes in flagella (Movassagh et al., 2010), *E. coli* chemoreceptors

(Khursigara et al., 2008), and for ER-bound ribosomes (Pfeffer et al., 2012). Finally, physiological changes at the cellular level may be described in detail by performing computer simulations of molecular pathways within a molecular environment that is precisely defined by cryo-ET (Beck et al., 2007; Khursigara et al., 2011).

Outlook

Cryo-ET stands out among imaging and structural biology methods. Because biological material is faithfully preserved by vitrification, molecular complexes are imaged in a fully hydrated, close-to-physiological state. Cryo-tomograms of intact cells are essentially snapshots of the entire cellular proteome at molecular resolution, which in principle enables mapping of the spatial relationships between macromolecules within the cell (Nickell et al., 2006). This includes the supramolecular architecture of transient complexes that are formed only under certain cellular conditions. In addition, the molecular crowding within cellular subvolumes, known to have profound effects on macromolecular interactions in living systems, can be investigated in a quantitative manner (Rigort et al., 2012a).

Paradoxically, the ability to visualize the complete molecular content of a system, one of the advantages of cryo-ET, significantly complicates the identification of individual molecular components within crowded cellular landscapes. Diverse identification strategies complementing cryo-ET with methods such as genetics and correlative fluorescence imaging are already in use and new approaches are being explored.

Sample thickness is a fundamental limitation of EM; it is a major obstacle to the applicability of EM and the achievable resolution. Because only a few cell types are sufficiently thin to be imaged intact, cellular cryo-ET requires preparative techniques that can provide controlled access to the insides of cells. FIB milling opens large windows into the cell's interior, enabling targeting of structural features within their natural cellular environments without violating their structural integrity. With vitrification providing the solution for sample preparation, controlling sample thickness by FIB milling will likely start another EM development cycle analogous to the one that was initiated more than 50 years ago by the development of ultramicrotomy.

Image-processing tools for uncovering high resolution information from cryo-tomograms, many of which are based on statistical methods, are becoming available and undergoing continuous development. Template matching aims to identify structures of interest in cryo-tomograms based on their structural signature, and may identify a significant number of molecular complexes in situ. Subtomogram averaging of sufficiently abundant larger assemblies reveals the high resolution structural information by averaging out noise. In conjunction with other methods, subtomogram averaging can provide pseudo-atomic structures of large complexes and discern different conformational and binding states.

These image-processing methods will become applicable to medium-sized and nonabundant proteins once the resolution of tomograms is improved. Current advancements in instrumentation may provide decisive steps in this direction. The increased sensitivity of new direct electron detectors makes more efficient use of the allowed electron exposure, increasing the SNR and the usable resolution. Phase plates still await the improvements necessary for widespread use, but they have the potential to improve both the high resolution information and the contrast of cryo-tomograms (see Box 2).

Cryo-ET is reaching the stage where it can provide comprehensive in situ molecular identification and attain high resolution information of deeply rooted functional modules that exist only in low-copy number and do not lend themselves to biochemical purification. Having already pushed the limits of imaging the undisturbed cellular interior, cryo-ET aims to bridge the gap between light microscopy and higher resolution methods such as x-ray crystallography and single-particle EM. The emergence of integrative approaches makes it possible to bring atomic resolution to in situ imaging. We expect that the electron microscope will again become a key instrument in cell biology by enabling the integration of structural data acquired at different-length scales.

References

Afzelius, B.A., and A.B. Maunsbach. 2004. Biological ultrastructure research; the first 50 years. *Tissue Cell.* 36:83–94. http://dx.doi.org/10.1016/j.tice.2003.11.001

Al-Amoudi, A., L.P. Norlen, and J. Dubochet. 2004. Cryo-electron microscopy of vitreous sections of native biological cells and tissues. *J. Struct. Biol.* 148:131–135. http://dx.doi.org/10.1016/j.jsb.2004.03.010

Al-Amoudi, A., D. Studer, and J. Dubochet. 2005. Cutting artefacts and cutting process in vitreous sections for cryo-electron microscopy. *J. Struct. Biol.* 150:109–121. http://dx.doi.org/10.1016/j.jsb.2005.01.003

Al-Amoudi, A., D.C. Díez, M.J. Betts, and A.S. Frangakis. 2007. The molecular architecture of cadherins in native epidermal desmosomes. *Nature.* 450:832–837. http://dx.doi.org/10.1038/nature05994

Alberts, B. 1998. The cell as a collection of protein machines: preparing the next generation of molecular biologists. *Cell.* 92:291–294. http://dx.doi.org/10.1016/S0092-8674(00)80922-8

Aloy, P., and R.B. Russell. 2004. Ten thousand interactions for the molecular biologist. *Nat. Biotechnol.* 22:1317–1321. http://dx.doi.org/10.1038/nbt1018

Ball, P. 2003. Portrait of a molecule. *Nature.* 421:421–422. http://dx.doi.org/10.1038/nature01404

Barber, C.F., T. Heuser, B.I. Carbajal-González, V.V. Botchkarev Jr., and D. Nicastro. 2012. Three-dimensional structure of the radial spokes reveals heterogeneity and interactions with dyneins in *Chlamydomonas* flagella. *Mol. Biol. Cell.* 23:111–120. http://dx.doi.org/10.1091/mbc.E11-08-0692

Beck, M., V. Lucić, F. Förster, W. Baumeister, and O. Medalia. 2007. Snapshots of nuclear pore complexes in action captured by cryo-electron tomography. *Nature.* 449:611–615. http://dx.doi.org/10.1038/nature06170

Beck, M., J.A. Malmström, V. Lange, A. Schmidt, E.W. Deutsch, and R. Aebersold. 2009. Visual proteomics of the human pathogen Leptospira interrogans. *Nat. Methods.* 6:817–823. http://dx.doi.org/10.1038/nmeth.1390

Braet, F., E. Wisse, P. Bomans, P. Frederik, W. Geerts, A. Koster, L. Soon, and S. Ringer. 2007. Contribution of high-resolution correlative imaging techniques in the study of the liver sieve in three-dimensions. *Microsc. Res. Tech.* 70:230–242. http://dx.doi.org/10.1002/jemt.20408

Brandt, F., L.A. Carlson, F.U. Hartl, W. Baumeister, and K. Grünewald. 2010. The three-dimensional organization of polyribosomes in intact human cells. *Mol. Cell.* 39:560–569. http://dx.doi.org/10.1016/j.molcel.2010.08.003

Branton, D. 1971. Freeze-etching studies of membrane structure. *Philos. Trans. R. Soc. Lond. B Biol. Sci.* 261:133–138. http://dx.doi.org/10.1098/rstb.1971.0043

Briegel, A., H.J. Ding, Z. Li, J. Werner, Z. Gitai, D.P. Dias, R.B. Jensen, and G.J. Jensen. 2008. Location and architecture of the Caulobacter crescentus

chemoreceptor array. *Mol. Microbiol.* 69:30–41. http://dx.doi.org/10.1111/j.1365-2958.2008.06219.x

Briegel, A., X. Li, A.M. Bilwes, K.T. Hughes, G.J. Jensen, and B.R. Crane. 2012. Bacterial chemoreceptor arrays are hexagonally packed trimers of receptor dimers networked by rings of kinase and coupling proteins. *Proc. Natl. Acad. Sci. USA.* 109:3766–3771. http://dx.doi.org/10.1073/pnas.1115719109

Briggs, J.A. 2013. Structural biology in situ-the potential of subtomogram averaging. *Curr. Opin. Struct. Biol.* 23:261–267. http://dx.doi.org/10.1016/j.sbi.2013.02.003

Bruggeller, P., and E. Mayer. 1980. Complete vitrification in pure liquid water and dilute aqueous solutions. *Nature.* 288:569–571. http://dx.doi.org/10.1038/288569a0

Bui, K.H., H. Sakakibara, T. Movassagh, K. Oiwa, and T. Ishikawa. 2009. Asymmetry of inner dynein arms and inter-doublet links in *Chlamydomonas* flagella. *J. Cell Biol.* 186:437–446. http://dx.doi.org/10.1083/jcb.200903082

Carnoy, J.B. 1884. La biologie cellulaire: étude comparée de la cellule dans les deux règnes. Joseph Van In & Co. 217 pp.

Crowther, R.A., D.J. DeRosier, and A. Klug. 1970. The reconstruction of a three-dimensional structure from projections and its application to electron microscopy. *Proc. R. Soc. Lond. A Math. Phys. Sci.* 317:319–340. http://dx.doi.org/10.1098/rspa.1970.0119

Cyrklaff, M., A. Linaroudis, M. Boicu, P. Chlanda, W. Baumeister, G. Griffiths, and J. Krijnse-Locker. 2007. Whole cell cryo-electron tomography reveals distinct disassembly intermediates of vaccinia virus. *PLoS ONE.* 2:e420. http://dx.doi.org/10.1371/journal.pone.0000420

Cyrklaff, M., C.P. Sanchez, N. Kilian, C. Bisseye, J. Simpore, F. Frischknecht, and M. Lanzer. 2011. Hemoglobins S and C interfere with actin remodeling in *Plasmodium falciparum*-infected erythrocytes. *Science.* 334:1283–1286. http://dx.doi.org/10.1126/science.1213775

Cyrklaff, M., C.P. Sanchez, F. Frischknecht, and M. Lanzer. 2012. Host actin remodeling and protection from malaria by hemoglobinopathies. *Trends Parasitol.* 28:479–485. http://dx.doi.org/10.1016/j.pt.2012.08.003

Danev, R., and K. Nagayama. 2010. Phase plates for transmission electron microscopy. *Methods Enzymol.* 481:343–369. http://dx.doi.org/10.1016/S0076-6879(10)81014-6

Denk, W., and H. Horstmann. 2004. Serial block-face scanning electron microscopy to reconstruct three-dimensional tissue nanostructure. *PLoS Biol.* 2:e329. http://dx.doi.org/10.1371/journal.pbio.0020329

Dierksen, K., D. Typke, R. Hegerl, A. Koster, and W. Baumeister. 1992. Towards automatic electron tomography. *Ultramicroscopy.* 40:71–87. http://dx.doi.org/10.1016/0304-3991(92)90235-C

Diestra, E., J. Fontana, P. Guichard, S. Marco, and C. Risco. 2009. Visualization of proteins in intact cells with a clonable tag for electron microscopy. *J. Struct. Biol.* 165:157–168. http://dx.doi.org/10.1016/j.jsb.2008.11.009

Dubochet, J., M. Adrian, J.J. Chang, J.C. Homo, J. Lepault, A.W. McDowall, and P. Schultz. 1988. Cryo-electron microscopy of vitrified specimens. *Q. Rev. Biophys.* 21:129–228. http://dx.doi.org/10.1017/S0033583500004297

Eltsov, M., K.M. Maclellan, K. Maeshima, A.S. Frangakis, and J. Dubochet. 2008. Analysis of cryo-electron microscopy images does not support the existence of 30-nm chromatin fibers in mitotic chromosomes in situ. *Proc. Natl. Acad. Sci. USA.* 105:19732–19737. http://dx.doi.org/10.1073/pnas.0810057105

Faas, F.G.A., M. Bárcena, A.V. Agronskaia, H.C. Gerritsen, K.B. Moscicka, C.A. Diebolder, L.F. van Driel, R.W.A.L. Limpens, E. Bos, R.B.G. Ravelli, et al. 2013. Localization of fluorescently labeled structures in frozen-hydrated samples using integrated light electron microscopy. *J. Struct. Biol.* 181:283–290. http://dx.doi.org/10.1016/j.jsb.2012.12.004

Fernandez, J.-J. 2012. Computational methods for electron tomography. *Micron.* 43:1010–1030. http://dx.doi.org/10.1016/j.micron.2012.05.003

Fernández, J.J., and S. Li. 2003. An improved algorithm for anisotropic nonlinear diffusion for denoising cryo-tomograms. *J. Struct. Biol.* 144:152–161. http://dx.doi.org/10.1016/j.jsb.2003.09.010

Fernández, J.J., S. Li, and R.A. Crowther. 2006. CTF determination and correction in electron cryotomography. *Ultramicroscopy.* 106:587–596. http://dx.doi.org/10.1016/j.ultramic.2006.02.004

Fernández-Busnadiego, R., B. Zuber, U.E. Maurer, M. Cyrklaff, W. Baumeister, and V. Lucic. 2010. Quantitative analysis of the native presynaptic cytomatrix by cryoelectron tomography. *J. Cell Biol.* 188:145–156. http://dx.doi.org/10.1083/jcb.200908082

Fernández-Busnadiego, R., S. Asano, A.-M. Oprisoreanu, E. Sakata, M. Doengi, Z. Kochovski, M. Zürner, V. Stein, S. Schoch, W. Baumeister, and V. Lucić. 2013. Cryo-electron tomography reveals a critical role of RIM1α in synaptic vesicle tethering. *J. Cell Biol.* 201:725–740. http://dx.doi.org/10.1083/jcb.201206063

Fernandez-Moran, H. 1953. A diamond knife for ultrathin sectioning. *Exp. Cell Res.* 5:255–256. http://dx.doi.org/10.1016/0014-4827(53)90112-8

Förster, F., O. Medalia, N. Zauberman, W. Baumeister, and D. Fass. 2005. Retrovirus envelope protein complex structure in situ studied by cryo-electron tomography. *Proc. Natl. Acad. Sci. USA.* 102:4729–4734. http://dx.doi.org/10.1073/pnas.0409178102

Förster, F., S. Pruggnaller, A. Seybert, and A.S. Frangakis. 2008. Classification of cryo-electron sub-tomograms using constrained correlation. *J. Struct. Biol.* 161:276–286. http://dx.doi.org/10.1016/j.jsb.2007.07.006

Frangakis, A.S., and R. Hegerl. 2001. Noise reduction in electron tomographic reconstructions using nonlinear anisotropic diffusion. *J. Struct. Biol.* 135:239–250. http://dx.doi.org/10.1006/jsbi.2001.4406

Frank, J. 2002. Single-particle imaging of macromolecules by cryo-electron microscopy. *Annu. Rev. Biophys. Biomol. Struct.* 31:303–319. http://dx.doi.org/10.1146/annurev.biophys.31.082901.134202

Fujiyoshi, Y. 2011. Electron crystallography for structural and functional studies of membrane proteins. *J. Electron Microsc. (Tokyo).* 60(Suppl 1):S149–S159. http://dx.doi.org/10.1093/jmicro/dfr033

Gan, L., and G.J. Jensen. 2012. Electron tomography of cells. *Q. Rev. Biophys.* 45:27–56. http://dx.doi.org/10.1017/S0033583511000102

Garvalov, B.K., B. Zuber, C. Bouchet-Marquis, M. Kudryashev, M. Gruska, M. Beck, A. Leis, F. Frischknecht, F. Bradke, W. Baumeister, et al. 2006. Luminal particles within cellular microtubules. *J. Cell Biol.* 174:759–765. http://dx.doi.org/10.1083/jcb.200606074

Gavin, A.-C., M. Bösche, R. Krause, P. Grandi, M. Marzioch, A. Bauer, J. Schultz, J.M. Rick, A.-M. Michon, C.-M. Cruciat, et al. 2002. Functional organization of the yeast proteome by systematic analysis of protein complexes. *Nature.* 415:141–147. http://dx.doi.org/10.1038/415141a

Geuze, H.J. 1999. A future for electron microscopy in cell biology? *Trends Cell Biol.* 9:92–93. http://dx.doi.org/10.1016/S0962-8924(98)01493-7

Glaeser, R.M. 2008. Retrospective: radiation damage and its associated "information limitations". *J. Struct. Biol.* 163:271–276. http://dx.doi.org/10.1016/j.jsb.2008.06.001

Glaeser, R., K. Downing, D. DeRosier, W. Chiu, and J. Frank. 2007. Electron Crystallography of Biological Macromolecules. Oxford University Press, Oxford, UK. 492 pp.

Guichard, P., A. Desfosses, A. Maheshwari, V. Hachet, C. Dietrich, A. Brune, T. Ishikawa, C. Sachse, and P. Gönczy. 2012. Cartwheel architecture of Trichonympha basal body. *Science.* 337:553. http://dx.doi.org/10.1126/science.1222789

Hartwell, L.H., J.J. Hopfield, S. Leibler, and A.W. Murray. 1999. From molecular to modular cell biology. *Nature.* 402):C47–C52. http://dx.doi.org/10.1038/35011540

Hayles, M.F., D.A.M. de Winter, C.T.W.M. Schneijdenberg, J.D. Meeldijk, U. Luecken, H. Persoon, J. de Water, F. de Jong, B.M. Humbel, and A.J. Verkleij. 2010. The making of frozen-hydrated, vitreous lamellas from cells for cryo-electron microscopy. *J. Struct. Biol.* 172:180–190. http://dx.doi.org/10.1016/j.jsb.2010.07.004

Henderson, R. 2004. Realizing the potential of electron cryo-microscopy. *Q. Rev. Biophys.* 37:3–13. http://dx.doi.org/10.1017/S0033583504003920

Heuser, J. 2002. Whatever happened to the 'microtrabecular concept'? *Biol. Cell.* 94:561–596. http://dx.doi.org/10.1016/S0248-4900(02)00013-8

Heuser, J.E., T.S. Reese, M.J. Dennis, Y. Jan, L. Jan, and L. Evans. 1979. Synaptic vesicle exocytosis captured by quick freezing and correlated with quantal transmitter release. *J. Cell Biol.* 81:275–300. http://dx.doi.org/10.1083/jcb.81.2.275

Heuser, T., M. Raytchev, J. Krell, M.E. Porter, and D. Nicastro. 2009. The dynein regulatory complex is the nexin link and a major regulatory node in cilia and flagella. *J. Cell Biol.* 187:921–933. http://dx.doi.org/10.1083/jcb.200908067

Hoffmann, C., A. Leis, M. Niederweis, J.M. Plitzko, and H. Engelhardt. 2008. Disclosure of the mycobacterial outer membrane: cryo-electron tomography and vitreous sections reveal the lipid bilayer structure. *Proc. Natl. Acad. Sci. USA.* 105:3963–3967. http://dx.doi.org/10.1073/pnas.0709530105

Hsieh, C.-E., A. Leith, C.A. Mannella, J. Frank, and M. Marko. 2006. Towards high-resolution three-dimensional imaging of native mammalian tissue: electron tomography of frozen-hydrated rat liver sections. *J. Struct. Biol.* 153:1–13. http://dx.doi.org/10.1016/j.jsb.2005.10.004

Humbel, B.M., M.D. de Jong, W.H. Müller, and A.J. Verkleij. 1998. Pre-embedding immunolabeling for electron microscopy: an evaluation of permeabilization methods and markers. *Microsc. Res. Tech.* 42:43–58. http://dx.doi.org/10.1002/(SICI)1097-0029(19980701)42:1<43::AID-JEMT6>3.0.CO;2-S

Hurbain, I., and M. Sachse. 2011. The future is cold: cryo-preparation methods for transmission electron microscopy of cells. *Biol. Cell.* 103:405–420. http://dx.doi.org/10.1042/BC20110015

Ingerson-Mahar, M., A. Briegel, J.N. Werner, G.J. Jensen, and Z. Gitai. 2010. The metabolic enzyme CTP synthase forms cytoskeletal filaments. *Nat. Cell Biol.* 12:739–746. http://dx.doi.org/10.1038/ncb2087

Khursigara, C.M., X. Wu, P. Zhang, J. Lefman, and S. Subramaniam. 2008. Role of HAMP domains in chemotaxis signaling by bacterial chemoreceptors. *Proc. Natl. Acad. Sci. USA*. 105:16555–16560. http://dx.doi.org/10.1073/pnas.0806401105

Khursigara, C.M., G. Lan, S. Neumann, X. Wu, S. Ravindran, M.J. Borgnia, V. Sourjik, J. Milne, Y. Tu, and S. Subramaniam. 2011. Lateral density of receptor arrays in the membrane plane influences sensitivity of the *E. coli* chemotaxis response. *EMBO J*. 30:1719–1729. http://dx.doi.org/10.1038/emboj.2011.77

Koning, R.I., S. Zovko, M. Bárcena, G.T. Oostergetel, H.K. Koerten, N. Galjart, A.J. Koster, and A. Mieke Mommaas. 2008. Cryo electron tomography of vitrified fibroblasts: microtubule plus ends in situ. *J. Struct. Biol.* 161:459–468. http://dx.doi.org/10.1016/j.jsb.2007.08.011

Koster, A.J., and J. Klumperman. 2003. Electron microscopy in cell biology: integrating structure and function. *Nat. Rev. Mol. Cell Biol.* 4(Suppl):SS6–SS10.

Koster, A.J., H. Chen, J.W. Sedat, and D.A. Agard. 1992. Automated microscopy for electron tomography. *Ultramicroscopy*. 46:207–227. http://dx.doi.org/10.1016/0304-3991(92)90016-D

Koster, A.J., R. Grimm, D. Typke, R. Hegerl, A. Stoschek, J. Walz, and W. Baumeister. 1997. Perspectives of molecular and cellular electron tomography. *J. Struct. Biol.* 120:276–308. http://dx.doi.org/10.1006/jsbi.1997.3933

Kudryashev, M., M. Cyrklaff, W. Baumeister, M.M. Simon, R. Wallich, and F. Frischknecht. 2009. Comparative cryo-electron tomography of pathogenic Lyme disease spirochetes. *Mol. Microbiol.* 71:1415–1434. http://dx.doi.org/10.1111/j.1365-2958.2009.06613.x

Kudryashev, M., M. Cyrklaff, R. Wallich, W. Baumeister, and F. Frischknecht. 2010a. Distinct in situ structures of the Borrelia flagellar motor. *J. Struct. Biol.* 169:54–61. http://dx.doi.org/10.1016/j.jsb.2009.08.008

Kudryashev, M., S. Lepper, R. Stanway, S. Bohn, W. Baumeister, M. Cyrklaff, and F. Frischknecht. 2010b. Positioning of large organelles by a membrane-associated cytoskeleton in *Plasmodium* sporozoites. *Cell. Microbiol.* 12:362–371. http://dx.doi.org/10.1111/j.1462-5822.2009.01399.x

Latta, H., and J.F. Hartmann. 1950. Use of a glass edge in thin sectioning for electron microscopy. *Proc. Soc. Exp. Biol. Med.* 74:436–439. http://dx.doi.org/10.3181/00379727-74-17931

Le Gros, M.A., G. McDermott, M. Uchida, C.G. Knoechel, and C.A. Larabell. 2009. High-aperture cryogenic light microscopy. *J. Microsc.* 235:1–8. http://dx.doi.org/10.1111/j.1365-2818.2009.03184.x

Li, Z., M.J. Trimble, Y.V. Brun, and G.J. Jensen. 2007. The structure of FtsZ filaments in vivo suggests a force-generating role in cell division. *EMBO J*. 26:4694–4708. http://dx.doi.org/10.1038/sj.emboj.7601895

Li, S., J.-J. Fernandez, W.F. Marshall, and D.A. Agard. 2012. Three-dimensional structure of basal body triplet revealed by electron cryo-tomography. *EMBO J*. 31:552–562. http://dx.doi.org/10.1038/emboj.2011.460

Lin, J., D. Tritschler, K. Song, C.F. Barber, J.S. Cobb, M.E. Porter, and D. Nicastro. 2011. Building blocks of the nexin-dynein regulatory complex in *Chlamydomonas* flagella. *J. Biol. Chem.* 286:29175–29191. http://dx.doi.org/10.1074/jbc.M111.241760

Liu, J., T. Lin, D.J. Botkin, E. McCrum, H. Winkler, and S.J. Norris. 2009. Intact flagellar motor of Borrelia burgdorferi revealed by electron cryo-tomography: evidence for stator ring curvature and rotor/C-ring assembly flexion. *J. Bacteriol.* 191:5026–5036. http://dx.doi.org/10.1128/JB.00340-09

Liu, J., B. Hu, D.R. Morado, S. Jani, M.D. Manson, and W. Margolin. 2012. Molecular architecture of chemoreceptor arrays revealed by cryoelectron tomography of *Escherichia coli* minicells. *Proc. Natl. Acad. Sci. USA*. 109:E1481–E1488. http://dx.doi.org/10.1073/pnas.1200781109

Lucić, V., F. Förster, and W. Baumeister. 2005a. Structural studies by electron tomography: from cells to molecules. *Annu. Rev. Biochem.* 74:833–865. http://dx.doi.org/10.1146/annurev.biochem.73.011303.074112

Lucić, V., T. Yang, G. Schweikert, F. Förster, and W. Baumeister. 2005b. Morphological characterization of molecular complexes present in the synaptic cleft. *Structure*. 13:423–434. http://dx.doi.org/10.1016/j.str.2005.02.005

Lucić, V., A.H. Kossel, T. Yang, T. Bonhoeffer, W. Baumeister, and A. Sartori. 2007. Multiscale imaging of neurons grown in culture: from light microscopy to cryo-electron tomography. *J. Struct. Biol.* 160:146–156. http://dx.doi.org/10.1016/j.jsb.2007.08.014

Mahamid, J., and W. Baumeister. 2012. Cryo-electron tomography: the realization of a vision. *Microscopy and Analysis*. 26:45–48.

Maimon, T., N. Elad, I. Dahan, and O. Medalia. 2012. The human nuclear pore complex as revealed by cryo-electron tomography. *Structure*. 20:998–1006. http://dx.doi.org/10.1016/j.str.2012.03.025

Marko, M., C. Hsieh, W. Moberlychan, C.A. Mannella, and J. Frank. 2006. Focused ion beam milling of vitreous water: prospects for an alternative to cryo-ultramicrotomy of frozen-hydrated biological samples. *J. Microsc.* 222:42–47. http://dx.doi.org/10.1111/j.1365-2818.2006.01567.x

Marko, M., C. Hsieh, R. Schalek, J. Frank, and C. Mannella. 2007. Focused-ion-beam thinning of frozen-hydrated biological specimens for cryo-electron microscopy. *Nat. Methods*. 4:215–217. http://dx.doi.org/10.1038/nmeth1014

Marsh, B.J., D.N. Mastronarde, K.F. Buttle, K.E. Howell, and J.R. McIntosh. 2001. Organellar relationships in the Golgi region of the pancreatic beta cell line, HIT-T15, visualized by high resolution electron tomography. *Proc. Natl. Acad. Sci. USA*. 98:2399–2406. http://dx.doi.org/10.1073/pnas.051631998

Martinez-Sanchez, A., I. Garcia, and J.-J. Fernandez. 2011. A differential structure approach to membrane segmentation in electron tomography. *J. Struct. Biol.* 175:372–383. http://dx.doi.org/10.1016/j.jsb.2011.05.010

Matricardi, V.R., R.C. Moretz, and D.F. Parsons. 1972. Electron diffraction of wet proteins: catalase. *Science*. 177:268–270. http://dx.doi.org/10.1126/science.177.4045.268

Maunsbach, A.B., and B.A. Afzelius. 1999. Biomedical Electron Microscopy. Academic Press. 548 pp.

McDowall, A.W., J.J. Chang, R. Freeman, J. Lepault, C.A. Walter, and J. Dubochet. 1983. Electron microscopy of frozen hydrated sections of vitreous ice and vitrified biological samples. *J. Microsc.* 131:1–9. http://dx.doi.org/10.1111/j.1365-2818.1983.tb04225.x

McMullan, G., S. Chen, R. Henderson, and A.R. Faruqi. 2009. Detective quantum efficiency of electron area detectors in electron microscopy. *Ultramicroscopy*. 109:1126–1143. http://dx.doi.org/10.1016/j.ultramic.2009.04.002

Medalia, O., I. Weber, A.S. Frangakis, D. Nicastro, G. Gerisch, and W. Baumeister. 2002. Macromolecular architecture in eukaryotic cells visualized by cryo-electron tomography. *Science*. 298:1209–1213. http://dx.doi.org/10.1126/science.1076184

Mercogliano, C.P., and D.J. DeRosier. 2007. Concatenated metallothionein as a clonable gold label for electron microscopy. *J. Struct. Biol.* 160:70–82. http://dx.doi.org/10.1016/j.jsb.2007.06.010

Milazzo, A.C., A. Cheng, A. Moeller, D. Lyumkis, E. Jacovetty, J. Polukas, M.H. Ellisman, N.H. Xuong, B. Carragher, and C.S. Potter. 2011. Initial evaluation of a direct detection device detector for single particle cryo-electron microscopy. *J. Struct. Biol.* 176:404–408. http://dx.doi.org/10.1016/j.jsb.2011.09.002

Moor, H., K. Muhlethaler, H. Waldner, and A. Frey-Wyssling. 1961. A new freezing-ultramicrotome. *J. Biophys. Biochem. Cytol.* 10:1–13. http://dx.doi.org/10.1083/jcb.10.1.1

Moussavi, F., G. Heitz, F. Amat, L.R. Comolli, D. Koller, and M. Horowitz. 2010. 3D segmentation of cell boundaries from whole cell cryogenic electron tomography volumes. *J. Struct. Biol.* 170:134–145. http://dx.doi.org/10.1016/j.jsb.2009.12.015

Movassagh, T., K.H. Bui, H. Sakakibara, K. Oiwa, and T. Ishikawa. 2010. Nucleotide-induced global conformational changes of flagellar dynein arms revealed by in situ analysis. *Nat. Struct. Mol. Biol.* 17:761–767. http://dx.doi.org/10.1038/nsmb.1832

Müller, H.R. 1957. [Freeze-drying as a fixation technic for plant cells]. *J. Ultrastruct. Res.* 1:109–137. http://dx.doi.org/10.1016/S0022-5320(57)80001-X

Newman, S.B., E. Borysko, and M. Swerdlow. 1949. New sectioning techniques for light and electron microscopy. *Science*. 110:66–68. http://dx.doi.org/10.1126/science.110.2846.66

Nicastro, D., X. Fu, T. Heuser, A. Tso, M.E. Porter, and R.W. Linck. 2011. Cryo-electron tomography reveals conserved features of doublet microtubules in flagella. *Proc. Natl. Acad. Sci. USA*. 108:E845–E853. http://dx.doi.org/10.1073/pnas.1106178108

Nickell, S., C. Kofler, A.P. Leis, and W. Baumeister. 2006. A visual approach to proteomics. *Nat. Rev. Mol. Cell Biol.* 7:225–230. http://dx.doi.org/10.1038/nrm1861

Nishino, Y., T. Yasunaga, and A. Miyazawa. 2007. A genetically encoded metallothionein tag enabling efficient protein detection by electron microscopy. *J. Electron Microsc. (Tokyo)*. 56:93–101. http://dx.doi.org/10.1093/jmicro/dfm008

Ortiz, J.O., F. Förster, J. Kürner, A.A. Linaroudis, and W. Baumeister. 2006. Mapping 70S ribosomes in intact cells by cryoelectron tomography and pattern recognition. *J. Struct. Biol.* 156:334–341. http://dx.doi.org/10.1016/j.jsb.2006.04.014

Ortiz, J.O., F. Brandt, V.R.F. Matias, L. Sennels, J. Rappsilber, S.H.W. Scheres, M. Eibauer, F.U. Hartl, and W. Baumeister. 2010. Structure of hibernating ribosomes studied by cryoelectron tomography in vitro and in situ. *J. Cell Biol.* 190:613–621. http://dx.doi.org/10.1083/jcb.201005007

Pfeffer, S., F. Brandt, T. Hrabe, S. Lang, M. Eibauer, R. Zimmermann, and F. Förster. 2012. Structure and 3D arrangement of endoplasmic reticulum membrane-associated ribosomes. *Structure*. 20:1508–1518. http://dx.doi.org/10.1016/j.str.2012.06.010

Pierson, J., U. Ziese, M. Sani, and P.J. Peters. 2011. Exploring vitreous cryo-section-induced compression at the macromolecular level using electron cryo-tomography; 80S yeast ribosomes appear unaffected. *J. Struct. Biol.* 173:345–349. http://dx.doi.org/10.1016/j.jsb.2010.09.017

Pigino, G., K.H. Bui, A. Maheshwari, P. Lupetti, D. Diener, and T. Ishikawa. 2011. Cryoelectron tomography of radial spokes in cilia and flagella. *J. Cell Biol.* 195:673–687. http://dx.doi.org/10.1083/jcb.201106125

Pilhofer, M., and G.J. Jensen. 2013. The bacterial cytoskeleton: more than twisted filaments. *Curr. Opin. Cell Biol.* 25:125–133. http://dx.doi.org/10.1016/j.ceb.2012.10.019

Porter, K.R., and H.S. Bennett. 1981. Introduction: recollections on the beginnings of the journal of cell biology. *J. Cell Biol.* 91:IX–XI.

Porter, K.R., and J. Blum. 1953. A study in microtomy for electron microscopy. *Anat. Rec.* 117:685–710. http://dx.doi.org/10.1002/ar.1091170403

Reimer, L., and H. Kohl. 2008. Transmission Electron Microscopy. Optical Sciences. Springer, Fifth ed. 590 pp.

Rigort, A., F.J. Bäuerlein, A. Leis, M. Gruska, C. Hoffmann, T. Laugks, U. Böhm, M. Eibauer, H. Gnaegi, W. Baumeister, and J.M. Plitzko. 2010. Micromachining tools and correlative approaches for cellular cryo-electron tomography. *J. Struct. Biol.* 172:169–179. http://dx.doi.org/10.1016/j.jsb.2010.02.011

Rigort, A., F.J.B. Bäuerlein, E. Villa, M. Eibauer, T. Laugks, W. Baumeister, and J.M. Plitzko. 2012a. Focused ion beam micromachining of eukaryotic cells for cryoelectron tomography. *Proc. Natl. Acad. Sci. USA.* 109:4449–4454. http://dx.doi.org/10.1073/pnas.1201333109

Rigort, A., D. Günther, R. Hegerl, D. Baum, B. Weber, S. Prohaska, O. Medalia, W. Baumeister, and H.-C. Hege. 2012b. Automated segmentation of electron tomograms for a quantitative description of actin filament networks. *J. Struct. Biol.* 177:135–144. http://dx.doi.org/10.1016/j.jsb.2011.08.012

Rigort, A., E. Villa, F.J.B. Bäuerlein, B.D. Engel, and J.M. Plitzko. 2012c. Integrative approaches for cellular cryo-electron tomography: correlative imaging and focused ion beam micromachining. *Methods Cell Biol.* 111:259–281. http://dx.doi.org/10.1016/B978-0-12-416026-2.00014-5

Robinson, C.V., A. Sali, and W. Baumeister. 2007. The molecular sociology of the cell. *Nature*. 450:973–982. http://dx.doi.org/10.1038/nature06523

Ruska, E. 1979. Die fruhe Entwicklung der Elektronenlinsen und der Elektronmikroskopie, *In* Acta historica leopoldina, Vol. 12. Deutsche Akademie der Naturforscher Leopoldina. 136 pp.

Salje, J., B. Zuber, and J. Löwe. 2009. Electron cryomicroscopy of *E. coli* reveals filament bundles involved in plasmid DNA segregation. *Science*. 323:509–512. http://dx.doi.org/10.1126/science.1164346

Sartori, A., R. Gatz, F. Beck, A. Rigort, W. Baumeister, and J. Plitzko. 2007. Correlative microscopy: bridging the gap between light- and cryo-electron microscopy. *J. Struct. Biol.* 160:135–145. http://dx.doi.org/10.1016/j.jsb.2007.07.011

Saxton, W.O., W. Baumeister, and M. Hahn. 1984. Three-dimensional reconstruction of imperfect two-dimensional crystals. *Ultramicroscopy*. 13:57–70. http://dx.doi.org/10.1016/0304-3991(84)90057-3

Schwartz, C.L., V.I. Sarbash, F.I. Ataullakhanov, J.R. McIntosh, and D. Nicastro. 2007. Cryo-fluorescence microscopy facilitates correlations between light and cryo-electron microscopy and reduces the rate of photobleaching. *J. Microsc.* 227:98–109. http://dx.doi.org/10.1111/j.1365-2818.2007.01794.x

Sjostrand, F.S. 1953. The ultrastructure of the innersegments of the retinal rods of the guinea pig eye as revealed by electron microscopy. *J. Cell. Physiol.* 42:45–70. http://dx.doi.org/10.1002/jcp.1030420104

Steere, R.L. 1957. Electron microscopy of structural detail in frozen biological specimens. *J. Biophys. Biochem. Cytol.* 3:45–60. http://dx.doi.org/10.1083/jcb.3.1.45

Studer, D., B.M. Humbel, and M. Chiquet. 2008. Electron microscopy of high pressure frozen samples: bridging the gap between cellular ultrastructure and atomic resolution. *Histochem. Cell Biol.* 130:877–889. http://dx.doi.org/10.1007/s00418-008-0500-1

Taylor, K.A., and R.M. Glaeser. 1974. Electron diffraction of frozen, hydrated protein crystals. *Science*. 186:1036–1037. http://dx.doi.org/10.1126/science.186.4168.1036

Tong, A.H.Y., G. Lesage, G.D. Bader, H. Ding, H. Xu, X. Xin, J. Young, G.F. Berriz, R.L. Brost, M. Chang, et al. 2004. Global mapping of the yeast genetic interaction network. *Science*. 303:808–813. http://dx.doi.org/10.1126/science.1091317

van Driel, L.F., J.A. Valentijn, K.M. Valentijn, R.I. Koning, and A.J. Koster. 2009. Tools for correlative cryo-fluorescence microscopy and cryo-electron tomography applied to whole mitochondria in human endothelial cells. *Eur. J. Cell Biol.* 88:669–684. http://dx.doi.org/10.1016/j.ejcb.2009.07.002

Vanhecke, D., S. Asano, Z. Kochovski, R. Fernandez-Busnadiego, N. Schrod, W. Baumeister, and V. Lučić. 2011. Cryo-electron tomography: methodology, developments and biological applications. *J. Microsc.* 242:221–227. http://dx.doi.org/10.1111/j.1365-2818.2010.03478.x

Verkleij, A.J., and P.H. Ververgaert. 1978. Freeze-fracture morphology of biological membranes. *Biochim. Biophys. Acta*. 515:303–327. http://dx.doi.org/10.1016/0304-4157(78)90017-5

Walther, T.C., and M. Mann. 2010. Mass spectrometry-based proteomics in cell biology. *J. Cell Biol.* 190:491–500. http://dx.doi.org/10.1083/jcb.201004052

Wang, Q., C.P. Mercogliano, and J. Löwe. 2011. A ferritin-based label for cellular electron cryotomography. *Structure*. 19:147–154. http://dx.doi.org/10.1016/j.str.2010.12.002

Zhang, P., C.M. Khursigara, L.M. Hartnell, and S. Subramaniam. 2007. Direct visualization of *Escherichia coli* chemotaxis receptor arrays using cryo-electron microscopy. *Proc. Natl. Acad. Sci. USA*. 104:3777–3781. http://dx.doi.org/10.1073/pnas.0610106104

Zuber, B., M. Chami, C. Houssin, J. Dubochet, G. Griffiths, and M. Daffé. 2008. Direct visualization of the outer membrane of mycobacteria and corynebacteria in their native state. *J. Bacteriol.* 190:5672–5680. http://dx.doi.org/10.1128/JB.01919-07